Ha *et al.*
Progress in Earth and Planetary Science (2026) 13:26
https://doi.org/10.1186/s40645-026-00813-y

Progress in Earth and Planetary Science

RESEARCH ARTICLE

Open Access

Validating tropospheric NO_2 column density from GEMS version 3.0 and Tropospheric Chemistry Reanalysis version 2 from background to urban conditions over Japan: with a focus on diurnal variations

Phuc Thi Minh Ha[1*], Yugo Kanaya[1], Takashi Sekiya[1], Hisahiro Takashima[2], Kengo Sudo[3], Yongjoo Choi[4], Limseok Chang[5], Hanlim Lee[6], Hyunkee Hong[5] and Jhoon Kim[7]

Abstract

This study validates tropospheric NO_2 vertical column density ($TropNO_2$ VCD) data from the Geostationary Environment Monitoring Spectrometer (GEMS) version 3.0 and the Tropospheric Chemistry Reanalysis version 2 (TCR-2) against Multi-Axis Differential Optical Absorption Spectroscopy (MAX-DOAS) and Tropospheric Monitoring Instrument (TROPOMI) data at three Japanese sites: Yokosuka (urban), Fukue (rural-remote), and Cape Hedo (remote). The GEMS v3.0 dataset showed markedly improved agreement with MAX-DOAS compared to v2.0, especially at Fukue and Cape Hedo remote islands, with significantly reduced normalized mean bias from 142–319% to 8–18%. GEMS v3.0 showed agreement with MAX-DOAS observations at Yokosuka ($R = 0.75$) and Fukue ($R = 0.50$). It performed particularly well in autumn and winter. There were positive biases in autumn at Yokosuka (NMB = 3.5%), but negative biases in the other seasons (NMB = −0.4% to −51.2%). The reanalysis TCR-2 and aggregated TROPOMI $TropNO_2$ VCD data (both at $1 \times 1°$ resolution) showed moderate to good correlation at all three sites ($R = 0.72$ at Yokosuka; $R = 0.44$ at Fukue; $R = 0.57$ at Cape Hedo). While the spatial resolution of TCR-2 ($1.1 \times 1.1°$) precluded meaningful comparisons with MAX-DOAS at urban sites such as Yokosuka, TCR-2 exhibited lower biases than TROPOMI at Cape Hedo, which represents a background environment (NMB = 38% vs. 87%). GEMS v3.0 data effectively captured midday NO_2 reductions at Cape Hedo, consistent with TCR-2 and MAX-DOAS, marking this as the first study to explore daytime NO_2 decreases in remote regions using GEMS. NO_2 loss pathways at Cape Hedo were examined using TCR-2 data and box-model simulations. NO_2 levels from GEMS exhibited a decline between 10 AM and 3 PM in autumn, aligning with patterns from MAX-DOAS and TCR-2, with NO_2 decay rates of 16 ± 10h from GEMS, 21 ± 5h from MAX-DOAS, and 22 ± 20h from TCR-2. The box-model NO_x budget analysis revealed that the $NO_2 + OH$ reaction was the dominant pathway for NO_x loss. The markedly improved agreement of GEMS v3.0 data with MAX-DOAS and TCR-2 data will allow potential exploration of the oxidizing capacity of the atmosphere over the clean marine regions, after further characterization of NO_x chemistry.

Keywords Nitrogen dioxide, Tropospheric chemistry, Satellite validation, GEMS, TROPOMI, TCR-2, MAX-DOAS, NO_x chemistry, Background environment, Photochemical processes

*Correspondence:
Phuc Thi Minh Ha
phucha@jamstec.go.jp
Full list of author information is available at the end of the article

1 Introduction

Nitrogen dioxide (NO_2), part of nitrogen oxides ($NO_x = NO + NO_2$), plays a crucial role in tropospheric chemistry. It controls the catalytic formation of O_3 and the oxidizing capacity of the atmosphere, represented by OH:

$$O_3 + h\nu \rightarrow O\left(^1D\right) + O_2(\lambda < 420nm) \quad \text{(R1)}$$

$$O\left(^1D\right) + H_2O \rightarrow 2OH \quad \text{(R2)}$$

$$H_2O + NO \rightarrow OH + NO_2 \quad \text{(R3)}$$

$$NO_2 + h\nu + O_2 \xrightarrow{N_2 or O_2} NO + O_3(\lambda < 420nm) \quad \text{(R4)}$$

The termination reaction occurs when NO_2 is oxidized to HNO_3:

$$OH + NO_2 + M \rightarrow HNO_3 + M \quad \text{(R5)}$$

The formed HNO_3 can be further converted to nitrates, which are supplied to the ocean as nutrients. This impacts the biogeochemistry and even the oceanic biological carbon pump (Honda et al. 2017; Yamaguchi et al. 2024).

Peroxyacetyl nitrate (PAN) is a secondary pollutant formed through photochemical reactions involving volatile organic compounds (VOCs) and affecting NO_x chemistry. Acetaldehyde (CH_3CHO) reacts with OH to form the peroxyacetyl (PA) radical, which then reacts with NO_2 to form PAN (Reactions R6 – 8). In the atmosphere, PAN acts as an important NO_x reservoir.

$$CH_3CHO + OH \rightarrow CH_3CO + H_2O \quad \text{(R6)}$$

$$CH_3CO + O_2 \rightarrow CH_3C(O)O_2 \quad \text{(R7)}$$

$$CH_3C(O)O_2 + NO_2 \leftrightarrow CH_3C(O)O_2NO_2 \quad \text{(R8)}$$

There are likely additional unknown NO_x-related chemical pathways, including the photolysis of nitrate and the formation of HONO (e.g., Kasibhatla et al. 2018), requiring more observational and process-oriented studies.

Satellite observations of NO_2 have advanced to facilitate the analysis of NO_x emission distribution and their temporal changes over decades (Burrows et al. 1999; Cifuentes et al. 2025; East et al. 2022; Jaeglé et al. 2005; Kim et al. 2020). However, despite the detection limit of TROPOMI with respect to $TropNO_2$ VCD being demonstrated to be approximately 1×10^{15} molecules/cm^2, the evaluation of these levels in the cleanest regions has been limited to data from the Fukue Island (32.75° N, 128.68° E) and Cape Hedo (26.87° N, 128.25° E) stations (see, for example, Fig. 36 of https://mpc-vdaf.tropomi.eu/ProjectDir/reports//pdf/S5P-MPC-IASB-ROCVR-24.00.00_FINAL_signed.pdf). Furthermore, the spatio-temporal distribution of these levels over the oceans has received scarce study. Kanaya et al. (2014) found that $TropNO_2$ VCD decreased during daytime over Cape Hedo in summer, in a manner similar to the decreases seen in the CHASER chemical transport model. They tentatively attributed this phenomenon to the oxidative loss of NO_2, but did not provide any further quantitative evaluation. With the launch in February 2020, a geostationary satellite instrument GEMS has become operational in Asia, possessing the capability to observe diurnal variations of atmospheric species such as NO_2, SO_2, O_3, HCHO. Despite the fact that probing the exceptionally low NO_2 levels is even more challenging from a geostationary orbit than from a lower sun-synchronous orbit, there are now opportunities to study NO_2 diurnal variations using GEMS and TROPOMI satellite-based data, ground-based remote sensing, and numerical model simulations in both clean and polluted regions.

Reanalysis is a systematic approach that provides long-term, observation-constrained datasets by assimilating multi-platform and multi-species measurements into chemical transport models, thereby overcoming the limitations of sparse observations. The TCR-2 dataset integrates multiple updated satellite observations of O_3, NO_2, and other species using the MIROC-CHASER model and an ensemble Kalman filter (EnKF) to optimize both chemical concentrations and precursor emissions. TCR-2 extends the earlier TCR-1 dataset (2005–2012; Miyazaki et al. 2015) and incorporates improvements in the EnKF data assimilation system (Miyazaki et al. 2019a), with validation against the KORUS-AQ aircraft campaign in 2016 (Miyazaki et al. 2019b) and shipborne measurements during 2012–2017 (Kanaya et al. 2019). The current version of the TCR-2 dataset has estimated NO_2 concentrations and NO_x emissions using the TROPOMI $TropNO_2$ VCD product (Miyazaki et al. 2021; Sekiya et al. 2022). However, the TCR-2 dataset has not been validated with ground-based MAX-DOAS remote sensing and GEMS $TropNO_2$ VCD product.

The present study initiates the validation of $TropNO_2$ VCD data from the satellite product GEMS version 3.0 and TCR-2 reanalysis data against ground-based MAX-DOAS and satellite TROPOMI measurements at three Japanese sites: Yokosuka (urban), Fukue (rural-remote), and Cape Hedo (remote). The GEMS and TCR-2 data are evaluated for their ability to capture diurnal variations in different pollution levels. A

case study on the NO_x loss processes in a clean environment will then be discussed. This discussion will be preceded by a postulation of the similarity between TCR-2, GEMS, and MAX-DOAS data at Cape Hedo in terms of the daytime reduction trends at midday in summer and autumn. A subsequent analysis of TCR-2 data, coupled with a NO_x-budget analysis by the 0-D box model version of the CHASER (MIROC-ESM) chemistry–climate model, successfully identifies the dominant NO_x loss pathways at midday in summer at Cape Hedo.

The following section details the methodologies and datasets employed. Section 3 presents the validation results for the GEMS version 3.0 TropNO_2 VCD product and TCR-2, using MAX-DOAS and TROPOMI as references. It also examines the nitrogen loss pathway at Cape Hedo at midday in summer and autumn. Finally, Sect. 4 presents the study's conclusions and key insights.

2 Methods

In this study, we utilize TropNO_2 VCD data and NO_2 concentrations to perform the analysis. This section provides information regarding the datasets used in Sect. 3.1, including satellite data from GEMS and TROPOMI, reanalysis TCR-2 data, and ground-based observations made by MAX-DOAS. The simulations by the 0-D box model used for Sect. 3.2 are also detailed. The domain of the GEMS and the locations of the MAX-DOAS instruments at the three sites in Japan are illustrated in Fig. 1.

2.1 Geostationary environment monitoring spectrometer (GEMS)

The GEMS instrument on the GEO-KOMPSAT 2B satellite was launched on February 18 and commenced operations since December 2020 (Kim et al. 2020, 2023). The satellite is situated at 128.2°E over the Equator, thereby encompassing a substantial portion of the Asian

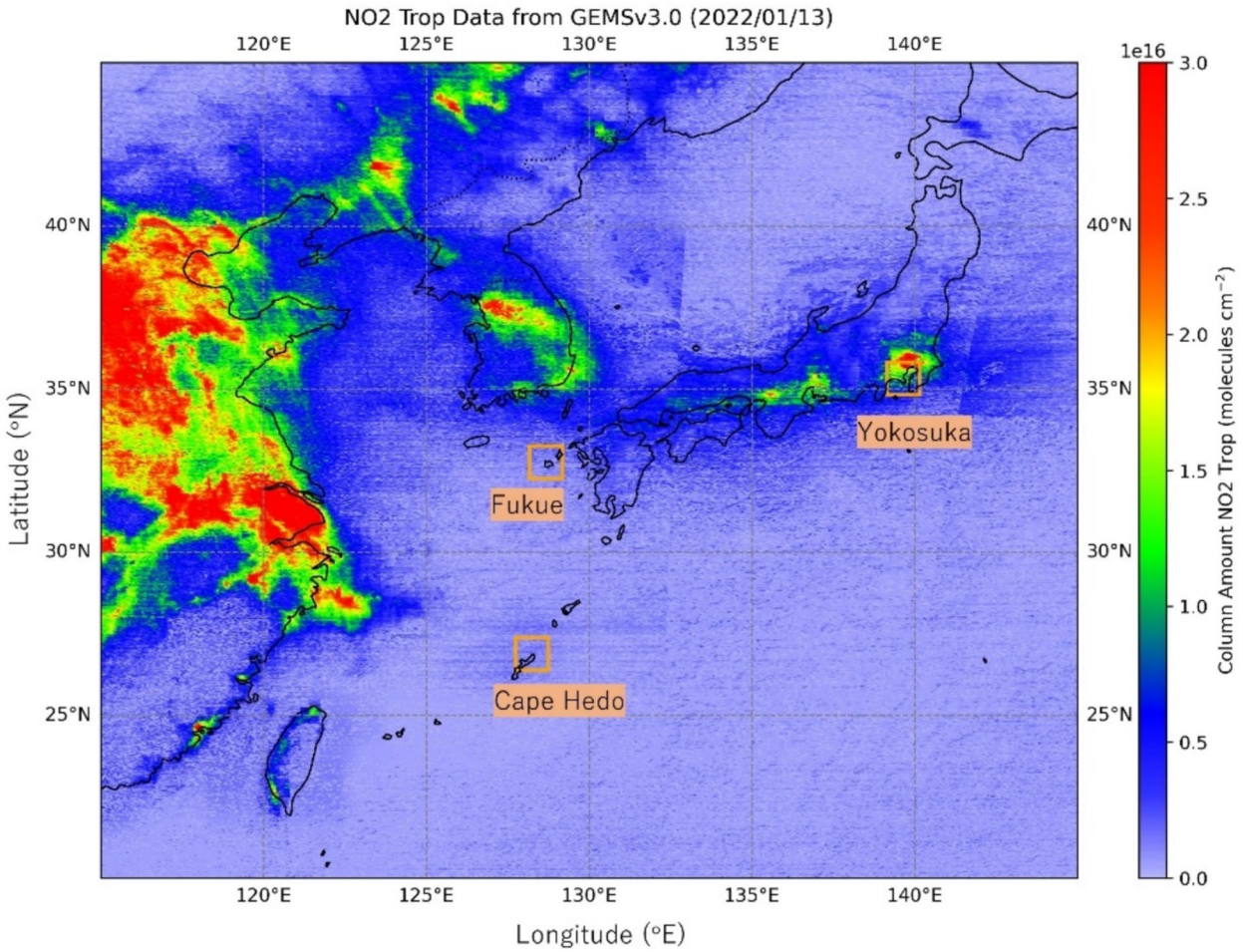

Fig. 1 GEMS TropNO_2 VCD (v3.0) retrieval before cloud- and quality-filtered, domain and locations of the three validation sites: Yokosuka, Fukue, Cape Hedo

continent (5°S–45°N and 75–145°E) with a nominal resolution of approximately 3.5 km × 8 km. GEMS v2.0 and v3.0 retrieve NO_2 in a fitting window of 432–450 nm with a spectral resolution of 0.6 nm (Kim et al. 2020). In the GEMS NO_2 algorithm, the air mass factor (AMF) look-up table (LUT) is constructed using monthly and hourly climatological Goddard Earth Observing System-Chem Model (GEOS-Chem) a priori data. GEMS employs four scan areas that progress from east to west: Half East (HE), Half Korea (HK), Full Central (FC), and Full West (FW). Each scan area is expected to be completed within 30 min, for example from 00:45 to 01:15 UTC. The current version (3.0) has been developed to enhance the accuracy of total, tropospheric, and stratospheric NO_2 columns in comparison with version 2.0. The comparison between versions 3.0 and 2.0 will be addressed in Sect. 3.1. This revision was achieved by modifying the AMF calculations, setting the tropopause to a fixed value of 230 hPa, and incorporating the most recent GEMS L2 aerosol (AERAOD), total O_3 (O3T), cloud (CLD), and background surface reflectance (BSR) data products. The implementation of AERAOD and O3T version 2.1, along with BSR and CLD version 3.0, ensures optimal consistency between the NO_2 products and the ozone, aerosol, and cloud data products (Lee et al. 2024).

The validation of GEMS NO_2 has been demonstrated through studies conducted on urban scales in China and South Korea (Kim et al. 2023; Lange et al. 2024), as well as through comparisons with Pandora observations and TROPOMI, using a deep learning approach to correct biases (Ghahremanloo et al. 2024). The GEMS data have also been used in a Bayesian inversion approach to update the NO_x emissions inventory in Asia (Park et al. 2024). However, it should be noted that all of these studies were conducted using either scientific GEMS NO_2 product versions or the operational GEMS L2 NO_2 v2.0 or earlier (i.e., not v3.0). These studies identified issues with v2.0, for example, the generally high biases in the Trop NO_2 VCD compared to ground-based and TROPOMI data, especially at non-urban sites.

In this study, hourly TropNO_2 VCD data from the revised GEMS L2 NO_2 v3.0 and v2.0 products, both spanning January 2022 to June 2024, are compared to evaluate improvements in v3.0. Data for the analysis were selected based on the following parameters: data within ± 0.05° grids of each MAX-DOAS site, a recording time of within ± 30 min of the site's recording time, a cloud fraction measurement below 0.3, and a Final Algorithm Flag value of zero (Table 1). GEMS data within ± 0.2° of the MAX-DOAS sites are utilized in Sect. 3.2 in order to increase data availability and statistical convergence, as compared to near-surface TCR-2 data (1.1 × 1.1°) at Cape Hedo. The current TropNO_2 VCD retrieval accuracy target is 1×10^{15} molecules/cm^2 (Kim et al. 2020), but this can be improved by statistical averaging, given that its uncertainty is primarily random (Platt and Stutz 2008). At Cape Hedo in summer, with 18 − 25 observations between 10 AM − 3 PM (with a measured value range as low as $(0.43 \pm 0.15) \times 10^{15}$ molecules/cm^2), the detection limit could be improved by a factor of ~ 4 − 5 at best, compared to a single measurement. Thus, an accuracy of ~ 0.25×10^{15} molecules/cm^2 was estimated

Table 1 The datasets employed in this study

	GEMS	MAX-DOAS	TROPOMI	TCR-2
Product	GEMS v2.0 NO_2, GEMS v3.0 L2 NO_2	Improved MAX-DOAS retrieval	TROPOMI/S5P NO_2 1-Orbit L2 Swath processor_version: 2.4.0	Reanalysis NO_2
Orbit type	Geosynchronous (nadir at 128°E)	Ground-based RS	Sun-synchronous (mean LST–13:35)	
NO_2 Fitting window spectral range	432 – 450 nm	460 – 490 nm	425 – 494 nm	
Spatial resolution	3.5 × 8 km		3.5 × 5.5 km	1 × 1° (~ 110 × 100 km)
Extract data at MAX-DOAS locations	± 0.05° (~ 11 × 10 km)		± 0.05° (~ 11 × 10 km)	
Time serries	1/2022 – 6/2024	1/2022–6/2024	1/2022 – 6/2024	7/2022 – 8/2023
Filter criteria	Cloud Fraction < 0.3, SZA < 85°, Final Algorithm Flags = 0	SZA < 85°, Totalflag = 0	qa value > 50%, Cloud Fraction < 0.3	surface to ~ 5 km
Chemistry-Transport Model (CTM) used	GEOS-Chem		TM5-MP (1 × 1°)	CHASER (MIROC)
References	Kim et al. 2020	Kanaya et al. 2014; Choi et al. 2021	https://sentiwiki.copernicus.eu/web/s5p-products; Veefkind et al. 2012	Miyazaki et al. 2020

at Cape Hedo, supporting the analysis of these low NO_2 levels.

2.2 Sentinel-5P tropospheric monitoring instrument (TROPOMI)

The TROPOMI/S5P NO_2 1-Orbit L2 Swath 5.5×3.5 km product, derived from the Tropospheric Monitoring Instrument (TROPOMI) integrated within the Sentinel-5 Precursor satellite, is utilized in this study. TROPOMI, which operates on a sun-synchronous orbit at an altitude of 824 km, is capable of providing high-resolution imaging; however, its observations are limited to daily snapshots in the early afternoon for mid-latitudes. The TROPOMI TropNO_2 VCD product has a spatial resolution of 5.5×3.5 km at nadir and a fitting window for NO_2 of 425–494 nm. Ground-based validation with global networks indicates markedly negative biases at polluted sites (Verhoelst et al. 2021). A comparison of TROPOMI NO_2 observations with the Copernicus Atmosphere Monitoring Service (CAMS) regional air quality ensemble revealed close agreement during summer and discrepancies during winter (Douros et al. 2023). Sekiya et al. (2022) showed that TROPOMI provides more accurate and consistent NO_2 measurements than OMI. This improvement results in more reliable global analyses of NO_2 and O_3 when TROPOMI is used instead of OMI in global chemical data assimilation.

For this study, TROPOMI/S5P TropNO_2 VCD data from 2022 to 2024 from collection 3 (version 2.4 or later versions) were acquired from the TEMIS website: https://www.temis.nl/airpollution/no2col/no2regio_tropomi.php. Low-quality pixels were filtered by applying a quality assurance threshold of below 0.5, which included cloud-covered scenes. For these scenes, only pixels with a cloud fraction > 0.3 were analyzed (Table 1). Using data with quality thresholds of 0.5 and 0.75 results in a 4–12% difference in data count, with no effect on bias, slope or correlation metrics relative to MAX-DOAS at the three sites.

2.3 Tropospheric chemistry reanalysis version 2 (TCR-2) data

The TCR-2 data (Miyazaki et al. 2020) were obtained by assimilating multiple satellite measurements. These included the OMI NO_2 QA4ECV v1.1 product (Boersma et al., 2017), the MLS v4.2 ozone and HNO_3 profiles (Livesey et al. 2018), the OMI PBL SO_2 product (Li et al. 2013), and the MOPITT v7 TIR/NIR CO product (Deeter et al. 2017). The TCR-2 system employed the Chemical Atmospheric General Circulation Model for Study of Atmospheric Environment and Radiative Forcing (CHASER) coupled with the Model for Interdisciplinary Research on Climate – Earth System Model (MIROC-ESM) with a resolution of 1.1°×1.1° and 32 vertical layers (Sudo et al. 2002; Sekiya et al. 2018), and a local ensemble transform Kalman filter technique with 32 ensemble members (LETKF, Hunt et al. 2007). This reanalysis has been validated against independent observations, including those from aircraft, satellites, and ozone sondes, thus demonstrating its reliability and consistency (Miyazaki et al. 2020). In this study, we extended the data assimilation calculation for July 2022-August 2023 using the TROPOMI NO_2 version 2.4 product (van Geffen et al. 2022) instead of OMI NO_2, as did in Miyazaki et al. (2021). To enable comparison with other datasets, we sampled the NO_2 profiles for the first nine layers (from ground to ~5 km altitude) at the observation sites and aggregated them. Due to the comparatively coarse resolution of TCR-2 data (1.1°×1.1°) compared to other datasets, aggregated TROPOMI data was utilized within the TCR-2 grid to enable more effective comparisons with TCR-2 data.

2.4 Multi-axis differential optical absorption spectroscopy (MAX-DOAS)

The MAX-DOAS instrument at Yokosuka (35.32° N, 139.65° E), designated as an urban site, Fukue (32.75° N, 128.68° E) as a rural to remote site, and Cape Hedo (26.87°N, 128.25°E) as a remote site, sequentially recorded scattered sunlight spectra from 300–550 nm at six elevation angles (3, 5, 10, 20, 30, and 90° (or 70° for Cape Hedo to avoid saturation)) using a rotating prism and a temperature-regulated spectrometer (Kanaya et al. 2014). The NO_2 fitting window was 460–490 nm. In this study, we employed data that were processed using an improved algorithm. In essence, the sequential retrieval approach involves firstly retrieving aerosols based on O_4 absorption features, followed by the NO_2 retrieval. The settings for the aerosol retrieval remain consistent with our original algorithm (Kanaya et al. 2014 and Choi et al. 2021). However, in the second step, the altitude layer depths for NO_2 to retrieve were refined (0–0.5 km, 0.5–1 km, 1–2 km, and 2–5 km) relative to the original (0–1 km, 1–2 km, 2–3 km, and 3–5 km) in order to optimize the utilization of observational data collected at near-horizontal angles. The state vector contained three parameters describing the NO_2 vertical profile besides TropNO_2 VCD: $\nu_{0-0.5\ km}$, $\nu_{0.5-1\ km}$, and $\nu_{1-2\ km}$. They are the fractions of NO_2 present in the given altitude layers out of the total but after removing the fractions in the lower layers. The a priori values and their respective uncertainties were optimized to 0.6 ± 0.4, 0.5 ± 0.4, 0.8 ± 0.2. These settings resulted in better agreement between the retrieved TropNO_2 VCD and the surface NO_2 concentrations at Yokosuka and the values obtained from a co-located Pandora146 spectrometer

and a surface NO_2 monitor (Kanaya et al., in preparation, 2025). The new retrieval results are hereafter simply referred to as MAX-DOAS. The dataset was further restricted to include only data with solar zenith angles (SZAs) of 85° (Table 1). MAX-DOAS TropNO_2 VCD measurements at Yokosuka exhibited a strong correlation with Pandora spectrometer results ($R^2 = 0.86$), with a MAX-DOAS/Pandora ratio of 1.04 ± 0.22 (1σ) (not shown). Combining the 4% systematic and 22% random uncertainties estimated from the comparison yielded an estimated total uncertainties of ± 22% for the MAX-DOAS TropNO_2 VCD. MAX-DOAS data at Cape Hedo during 10 AM–3 PM in 2022 show a median error of 7.42×10^{14} molecules/cm^2 for the differential slant column density of NO_2 at an elevation angle of 3 degrees (DSCD_3(NO_2)). Using the typical enhancement ratio of DSCD_3(NO_2) to TropNO_2 VCD of 4.9, the TropNO_2 VCD detection limit from MAX-DOAS was estimated to be 3.0×10^{14} molecules/cm^2 with a signal-to-noise ratio of 2 for a single observation. The proportion of MAX-DOAS data above this threshold was found to be 90.1% at Cape Hedo, 99.8% at Fukue, and 100% at Yokosuka. TropNO_2 VCD as low as $1.3 - 5 \times 10^{14}$ molecules/cm^2 were also detectable over remote oceans by MAX-DOAS and satellite instruments (Peters et al. 2012, Wang et el., 2020). Given the naturally low NO_2 levels at Cape Hedo and the absence of explicit detection limits for TropNO_2 VCD retrievals in this study, high-quality low-TropNO_2 VCD data are retained for analysis. It is important to note that Cape Hedo has served as a critical observational site for satellite validation for decades, particularly within the lowest range of tropospheric NO_2 column (e.g., https://mpc-vdaf.tropomi.eu/ProjectDir/reports//pdf/S5P-MPC-IASB-ROCVR-24.00.00_FINAL_signed.pdf). In this study, we seek to assess GEMS NO_2 products at such low NO_2 levels for the first time.

2.5 0-D box model version of the CHASER (MIROC-GSM).

The zero-dimensional (0-D) box model is a valuable tool for understanding chemical processes, testing hypotheses through sensitivity simulations and comparisons with observations (Wolfe et al. 2016), and analyzing laboratory experiments (Coates and Butler 2015; Stone et al. 2011; Paulot et al. 2009).

In this study, we used the 0-D box model version of the CHASER/MIROC-ESM (Sudo et al. 2002; Sudo and Akimoto 2007; Watanabe et al. 2011), to conduct chemical simulations for a typical clean environment similar to Cape Hedo (Sect. 3.2). The box model includes identical chemical components to its 3-D model, encompassing the O_x-HO_x-NO_x-CH_4-CO photochemical system and oxidation of nonmethane hydrocarbons through 262 chemical reactions with 92 chemical species. Its 3-D model evaluations have been extensively reported in the literature (e.g., Ha et al. 2021, 2023; He et al. 2022; Hoque et al. 2024). However, the 0-D box-model does not account for vertical and horizontal transport, emission sources, dry and wet deposition, or meteorological processes. Instead, the focus is on chemical processes and their equilibrium.

In this study, we performed a simulation of a clean environment resembling Cape Hedo, using initial concentrations derived from the 3D CHASER model. NO_x emissions were set to align with observed NO_x concentrations at Cape Hedo (350–600 ppt). It should be noted that aerosol concentrations were not included in this simulation, and the photolysis frequency values incorporated diurnal cycles that suppose sunrise at 6 AM and sunset at 6 PM, but does not consider SZA at the given specific location and time. A detailed NO_x budget analysis was carried out over 7 days in the middle of a 14-day simulation to avoid the spin-up period and ensure flux stability. This analysis included 49 NO_x-related reactions and focused on midday NO_x loss (10 AM–3 PM) to evaluate the contributions of individual loss pathways.

2.6 NO_2 vertical profile preprocessing

The MAX-DOAS vertical grid consists of 51 layers, extending from the surface to 5000 m. For Yokosuka, layer 1 spans 0–10 m (thickness: 10 m), layer 2 spans 10–100 m (thickness: 90 m), layer 3 spans 100–200 m (thickness: 100 m), and layers 4 − 51 have a uniform thickness of 100 m. For Fukue, layer 1 spans 80–86 m (thickness: 6 m), layer 2 spans 86–100 m (thickness: 14 m), layers 3 and above have the same vertical structure as Yokosuka. For Cape Hedo, layer 1 spans 0–68 m (thickness: 68 m), layer 2 spans 68–100 m (thickness: 32 m), layers 3 and above are identical to those used for Yokosuka.

GEMS provides vertical pressure information across 47 retrieval layers, spanning approximately from 1000 to 0 hPa. For this study, we used the lowest 23 layers, corresponding to altitudes from the surface up to ~ 5000 m. The partial column of NO_2 in each layer was calculated by scaling the a priori NO_2 profile:

$$PartialcolumnNO_2^{(i)} = \left(\frac{AprioriNO_2^{(i)}}{\sum_{j=1}^{23} AprioriNO_2^{(j)}} \right) \times PosterioriTropNO_2VCD$$

The NO_2 partial column was weighted by air density and pressure, subsequently interpolated onto the 51-layer vertical grid used in MAX-DOAS retrievals to enable consistent comparison.

For the TCR-2 vertical profile, the NO_2 partial column concentration for the first nine layers (corresponding to the surface up to ~ 5000 m) was extracted and redistributed in a similar way onto the 51-layer MAX-DOAS grid using pressure-weighting (Table 2).

3 Results and discussion

3.1 Comparing TropNO_2 VCD across datasets

In this section, TropNO_2 VCD from multiple platforms will be compared, aiming to evaluate the performance of GEMS and TCR-2 against MAX-DOAS and TROPOMI TropNO_2 VCD data, which are widely regarded as reliable and consistent (Kanaya et al. 2014; Douros et al. 2023; Verhoelst et al. 2021; Sekiya et al. 2022).

Figure 2, which incorporates all daytime data coinciding with MAX-DOAS observations, demonstrates substantial improvements of GEMS v3.0 over v2.0 in terms of seasonal agreement with MAX-DOAS across all three locations, but particularly at Fukue and Cape Hedo. The data statistical metrics presented in Table 3 show an increase in the correlation coefficients (R), rising from 0.63 to 0.75 at Yokosuka. In addition, there was a significant reduction in mean bias errors (MBE) at Fukue and Cape Hedo, with values decreasing from 2.49 – 2.69 to (−0.05)–(−0.28)) × 10^{15} molecules/cm^2, and the normalized mean bias (NMB) decreased from 142–319% to 8–18%. These improvements in version 3.0 may be due to modifications in the AMF calculations and the stratosphere-troposphere separation process, which impact remote sites more than urban areas.

The monthly mean GEMS v3.0 data clearly depict seasonal variations at Yokosuka and Fukue, with MAX-DOAS peaking during winter months at Yokosuka. Data at Cape Hedo show nearly no seasonal variation in NO_2, with the MAX-DOAS recording approximately 0.5 – 1.0 × 10^{15} molecules/cm^2, although there is a tendency toward slightly lower NO_2 levels in summer across all datasets. GEMS v3.0 demonstrated satisfactory performance in Yokosuka and Fukue; however, it did not reach the performance level of TROPOMI (R_{GEMS} = 0.75 vs. $R_{TROPOMI}$ = 0.90 at Yokosuka and R_{GEMS} = 0.50 vs. $R_{TROPOMI}$ = 0.61 at Fukue). This discrepancy can be attributed in part to the weaker performance of GEMS in the morning (later discussion in Sect. 3.1.2) relative to its stronger performance in the afternoon and around the TROPOMI overpass time (addressed subsequently in Sect. 3.1.1).

The TCR-2 TropNO_2 VCD is lower than the MAX-DOAS TropNO_2 VCD at Yokosuka because the low horizontal resolution of TCR-2 (1.1° × 1.1°) leads to a poor representation of elevated NO_2 levels in urban areas. TCR-2 NO_2 data are more comparable with NO_2 from MAX-DOAS and GEMS at Fukue and Cape Hedo. As demonstrated in the scatter plots of Fig. 2 and the statistical metrics in Table 3, hourly TCR-2 versus MAX-DOAS data revealed a regression line slope b of 1.80 ± 0.09 with a lower bias (NMB = 38%) for Cape Hedo, which were higher by TROPOMI (slope = 3.84 ± 0.60, NMB = 87%). At Cape Hedo, there is a strong positive correlation between the columns of TCR-2 and MAX-DOAS, although the correlation coefficients are not particularly high. Given the low levels of NO_2, high hourly correlations are not a viable expectation.

When examining the selected data matching the TROPOMI overpass time (i.e., periods during which hourly TROPOMI data was available) (Fig. 3c), TCR-2 successfully reproduced the low NO_2 levels in summer at Cape Hedo, as detected by MAX-DOAS and GEMS (~ 0.5 × 10^{15} molecules/cm^2). In contrast, TROPOMI exhibited a consistent positive bias, approximately a factor of two. Given the coarser resolution of TCR-2 compared to the other datasets, the comparison accuracy was enhanced by aggregating the hourly TropNO_2 VCD data from TROPOMI to the TCR-2 horizontal grid resolution (1.1° × 1.1°) (Fig. 4). Compared to Figure S5, the correlation coefficients and slope values both increase: Yokosuka (R from 0.45 to 0.72, slope from 0.45 to 1.04), Fukue (R from 0.34 to 0.44, slope from 0.60 to 0.83), and Cape Hedo (R from 0.42 to 0.57). The TCR-2 results indicate a slight positive bias relative to TROPOMI at Yokosuka (MBE = 1.27 × 10^{15} molecules/cm^2), and negligible but negative biases at Fukue (MBE = -0.17 × 10^{15} molecules/cm^2) and Cape Hedo (MBE = -0.08 × 10^{15} molecules/cm^2).

Table 2 NO_2 and NO_x decay rates (τ, hours) during midday near-surface layer (0–100 m; 10 AM–3 PM) in summer and autumn

	τ (hr) in summer	τ (hr) in autumn
MAX-DOAS	17 ± 8	21 ± 5
GEMS (± 0.05°)	/	8 ± 2
GEMS (± 0.2°)	/	16 ± 10
TCR-2	30 ± 8	22 ± 20
TCR-2 (NO_x)	26 ± 6	25 ± 26

3.1.1 Seasonality

Figure 5 presents scatter plots of hourly TropNO_2 VCD data from GEMS, TROPOMI, and TCR-2 versus MAX-DOAS at Yokosuka and Fukue + Cape Hedo for each season. The statistical metrics are listed in Tables 4 for Yokosuka and Table S1 for Fukue + Cape Hedo. GEMS v3.0 performed very well against MAX-DOAS in autumn and winter, with correlation coefficients of 0.80 at Yokosuka (Fig. 5g and h) and 0.60 – 0.66 at Fukue and Cape Hedo (Fig. 5c and d). The slopes of the regression lines

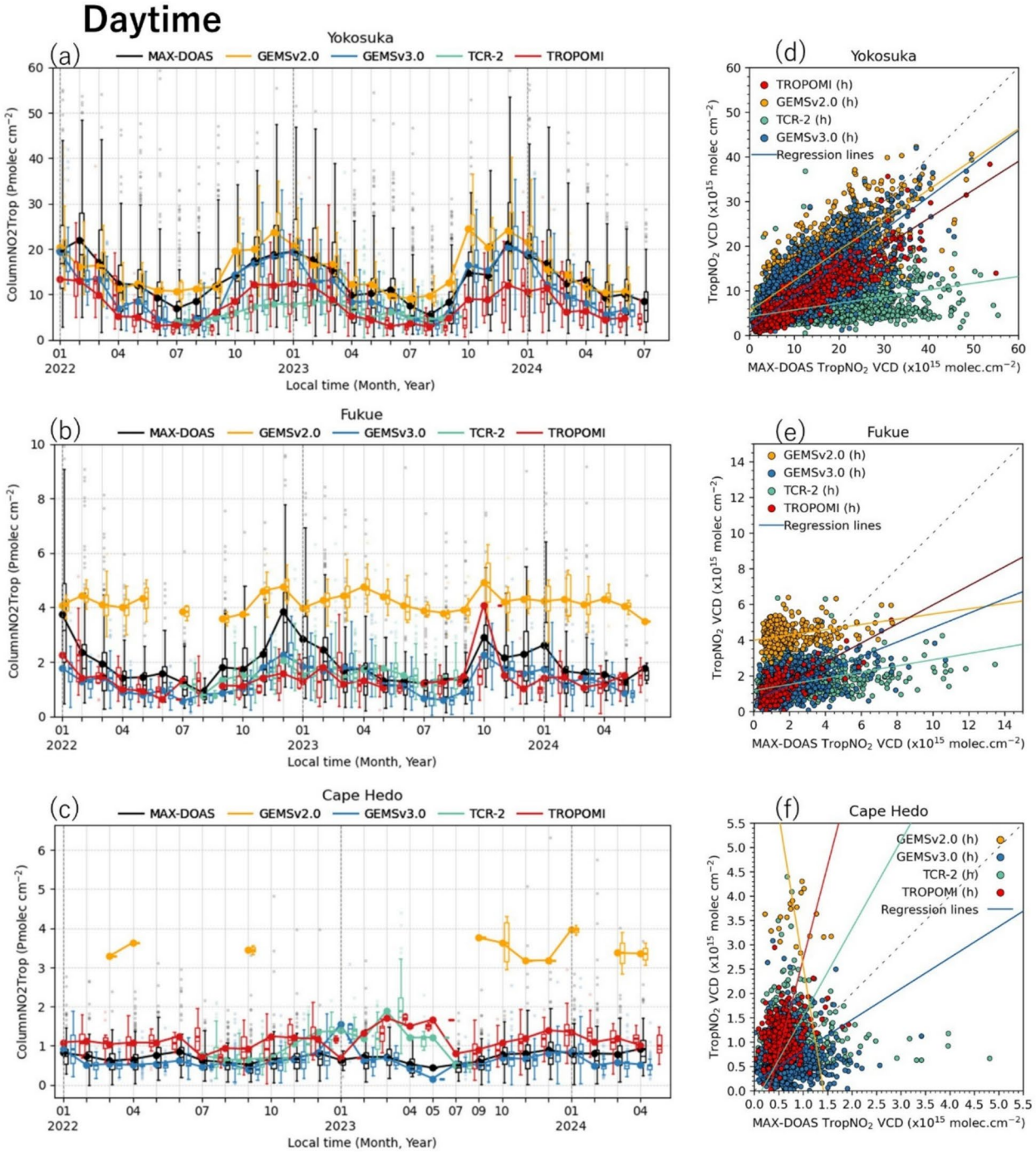

Fig. 2 Time-series and scatter plots for $TropNO_2$ VCD during all daytime **a**, **d** at Yokosuka, **b**, **e** at Fukue, and **c**, **f** at Cape Hedo. Panels (**a**, **b**, **c**) display monthly mean values from MAX-DOAS (all data; black), GEMS v2.0 (orange), GEMS v3.0 (blue), TCR-2 (cyan); these three datasets showed data coincident with MAX-DOAS observations; and TROPOMI (one measurement per day; red). The boxes represent the interquartile range (IQR) of each dataset, and the whiskers extend to 1.5 times the IQR from the quartiles. Thin dashed lines indicate median values of each hourly dataset, with outliers plotted as individual points. Panels (**d**, **e**, **f**) show scatter plots for hourly data from GEMS v2.0 (orange), GEMS v3.0 (blue), TROPOMI (red), and TCR-2 (cyan) versus MAX-DOAS. Statistical metrics of these plots are displayed in Tables 3. All analyses have P values < 0.05

Table 3 Statistical metrics for TropNO_2 VCD data at the three validation locations. Metrics include Y-intercept (a, $\times 10^{15}$ molecules/cm^2), the regression line slope (b), the correlation coefficients (*R*), the data counts (*N*), the mean bias error (MBE, $\times 10^{15}$ molecules/cm^2), and the normalized mean bias (NMB, %). These metrics correspond to the scatter plots of GEMS v2.0, GEMS v3.0, TROPOMI, and TCR-2, compared with MAX-DOAS in Fig. 2. Underlined values are referenced in the text

	GEMSv2	GEMSv3	TROPOMI	TCR-2
Yokosuka				
a	5.47 ± 0.38	1.36 ± 0.23	0.92 ± 0.17	4.2 ± 0.07
b	0.68 ± 0.02	0.74 ± 0.01	0.62 ± 0.01	0.15 ± 0.005
R	0.63	0.75	0.90	0.44
N	1052	1602	561	3530
MBE	0.19	−2.14	−3.53	−5.80
NMB (%)	1.2	−15.8	−30.5	−49.3
Fukue				
a	4.00 ± 0.05	0.66 ± 0.03	0.62 ± 0.06	1.17 ± 0.02
b	0.15 ± 0.02	0.40 ± 0.02	0.54 ± 0.04	0.17 ± 0.01
R	0.27	0.50	0.61	0.35
N	380	1305	227	1873
MBE	2.49	−0.28	−0.02	−0.39
NMB (%)	141.5	−17.8	−1.6	−20.7
Cape Hedo				
a	8.76 ± 6.7	0.19 ± 0.03	−1.14 ± 0.35	−0.26 ± 0.06
b	−6.19 ± 7.91	0.64 ± 0.04	3.84 ± 0.60	1.80 ± 0.09
R	0.06	0.08	0.23	0.18
N	19	1319	275	1331
MBE	2.69	−0.05	0.51	0.23
NMB (%)	318.6	−7.8	87.5	37.7

with MAX-DOAS at Yokosuka are 0.76 in autumn and 0.66 in winter, closer to unity than the slope of TROPOMI (0.62 in autumn and 0.60 in winter), as shown in Table 4. However, GEMS exhibits a positive bias at Yokosuka in autumn (MBE = 0.47×10^{15} molecules/cm^2, NMB = 3.5%), while negative biases in other seasons (NMB = −0.4% in winter, −29.5% in spring, and −51.2% in summer) (Table 4). The large biases in GEMS observations at Yokosuka in summer may be attributed to its poor performance in summer mornings (to be discussed in Sect. 3.1.2), and the unavailability of afternoon data. Due to diurnal bias variation in GEMS, the seasonality in GEMS is different from TROPOMI, which shows no clear seasonality at Yokosuka in terms of regression slopes and their biases. TCR-2 do not perform well at Yokosuka due to its coarse horizontal resolution of 1.1° × 1.1°.

At Fukue and Cape Hedo, the correlation of GEMS is poor in the summer (*R* = 0.15) with high NMB (−29%). The strong seasonal differences in GEMS bias may be related to its ability to capture near-surface data between 10 AM – 1 PM, particularly during the early morning peak in NO_2 levels as observed by MAX-DOAS. This ability may be less favorable in spring and especially in summer (higher solar elevation), than in autumn and winter. For TROPOMI, it exhibits substantial biases during summer and autumn (NMB = 57 – 68%, Table S1) at Fukue and Cape Hedo. This is due to the different seasonal biases at Fukue and Cape Hedo compensating for each other. For instance, the low bias in winter for the Fukue + Cape Hedo group (NMB = 6.6%, Table S1) results from a negative bias at Fukue (NMB = -19.4%) and a pronounced positive bias at Cape Hedo (NMB = +97.9%) (data not shown; see Fig. 6h, l). Another study reported mostly negative biases of TROPOMI against MAX-DOAS, but also noted a tendency toward positive bias in cleaner conditions (Verhoelst et al. 2021). This tendency aligns with our results at all three sites: negative biases of TROPOMI at Yokosuka and in winter at Fukue, and positive biases at Cape Hedo and other seasons at Fukue. In contrast to TROPOMI at Fukue and Cape Hedo, TCR-2 demonstrates regression slopes closer to unity, higher correlation coefficients, and lower biases in summer and autumn, although it has large negative bias in winter (NMB = −31%). This may be due to stronger NO_2 transport from continental sources (e.g., China) to Fukue in winter, which the coarse resolution of TCR-2 fails to capture locally.

A comparison of GEMS, TROPOMI, and TCR-2 data with MAX-DOAS confined to the TROPOMI overpass time are shown in Figure S1, and the statistical metrics of these scatter plots are shown in Tables S2 and S3. Limiting GEMS observations to the TROPOMI overpass time shows comparable or slightly better regression slopes and correlation coefficients, as well as smaller biases, in spring at Yokosuka (MBE = $(-3.8 \rightarrow -1.6) \times 10^{15}$ molecules/cm^2, NMB = −30% → −19%). In winter, however, the bias increases slightly. In other seasons, data are scarce due to the site lying outside the GEMS scan area during afternoon (Tables 4 and S2). At Fukue + Cape Hedo, GEMS data at TROPOMI overpass time shows relatively similar regression slopes and *R* values to GEMS data at MAX-DOAS observation time across all seasons, except in summer when data are limited (Tables S1 and S3). Furthermore, GEMS biases are largely mitigated in all seasons when confined to the TROPOMI overpass time (NMB = 6 – 29% → 2 – 4%), except in winter. The enhanced performance of GEMS at TROPOMI overpass time is consistent with that of the prior version (v2.0) when evaluated against ground-based data from South Korea (Lange et al. 2024), although GEMS data are limited at our locations in certain seasons. For TCR-2 at Fukue and Cape Hedo, good performance in summer and autumn is preserved when confined to TROPOMI overpass time, with slightly reduced biases (NMB from 5% to

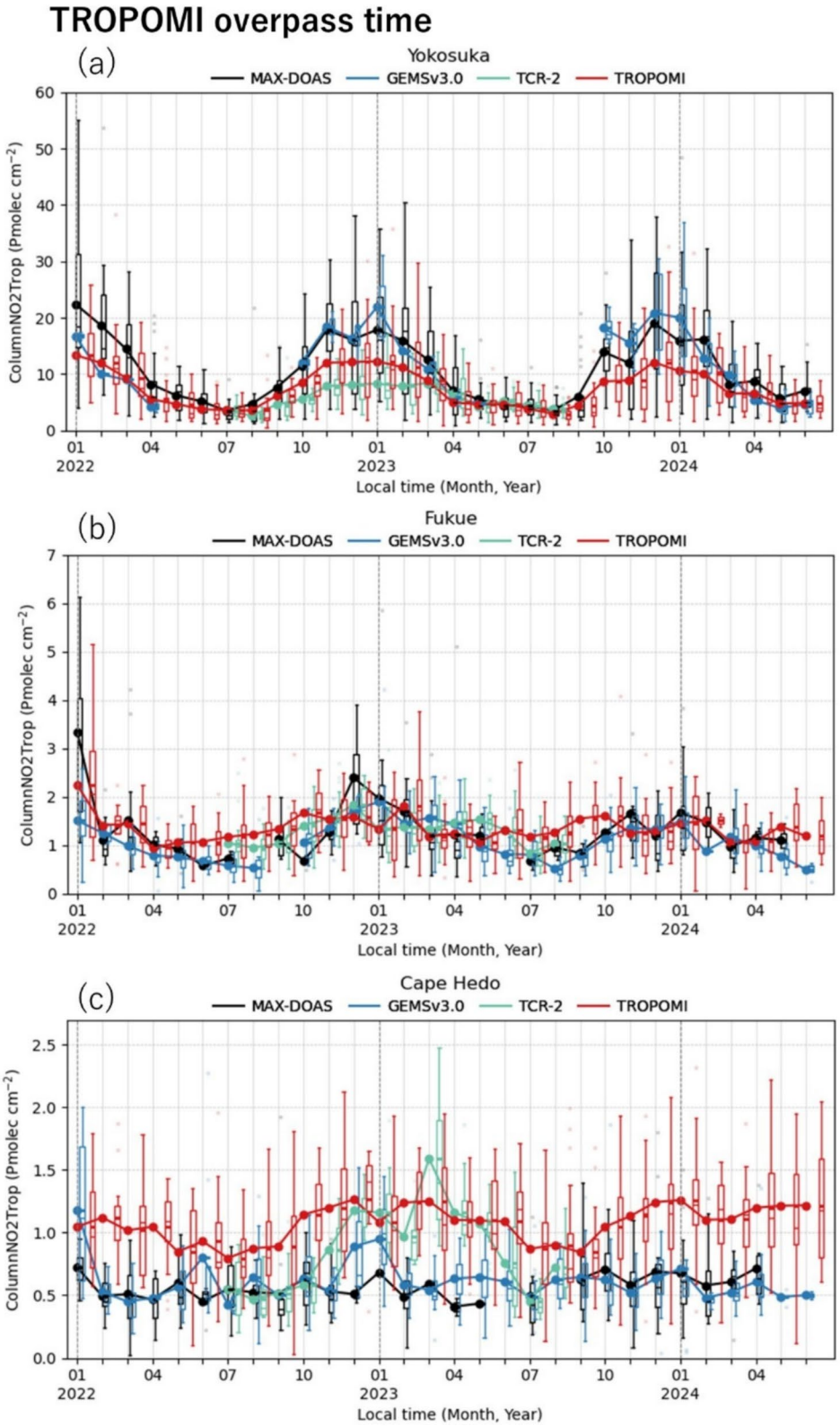

Fig. 3 Time-series of TropNO_2 VCD during TROPOMI overpass times, with legends consistent with Fig. 2a, b, and c, excluding any reference to GEMS v2.0 data

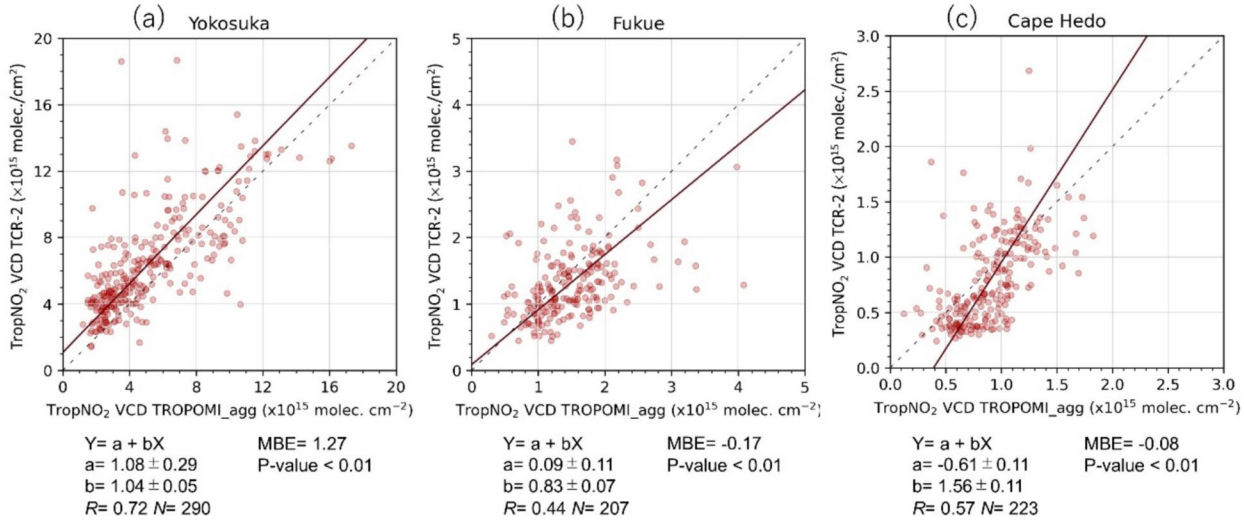

Fig. 4 Scatter plots of hourly data of $TropNO_2$ VCD from TCR-2 and TROPOMI. TROPOMI data are aggregated at TCR-2 horizontal grid resolution (1.1°). Statistical values including the Y-intercept (a, $\times 10^{15}$ molecules/cm^2), slope of regression lines of the scatter plots (b), correlation coefficients (*R*), number of data (*N*), mean bias error (MBE, $\times 10^{15}$ molecules/cm^2), and P values are shown

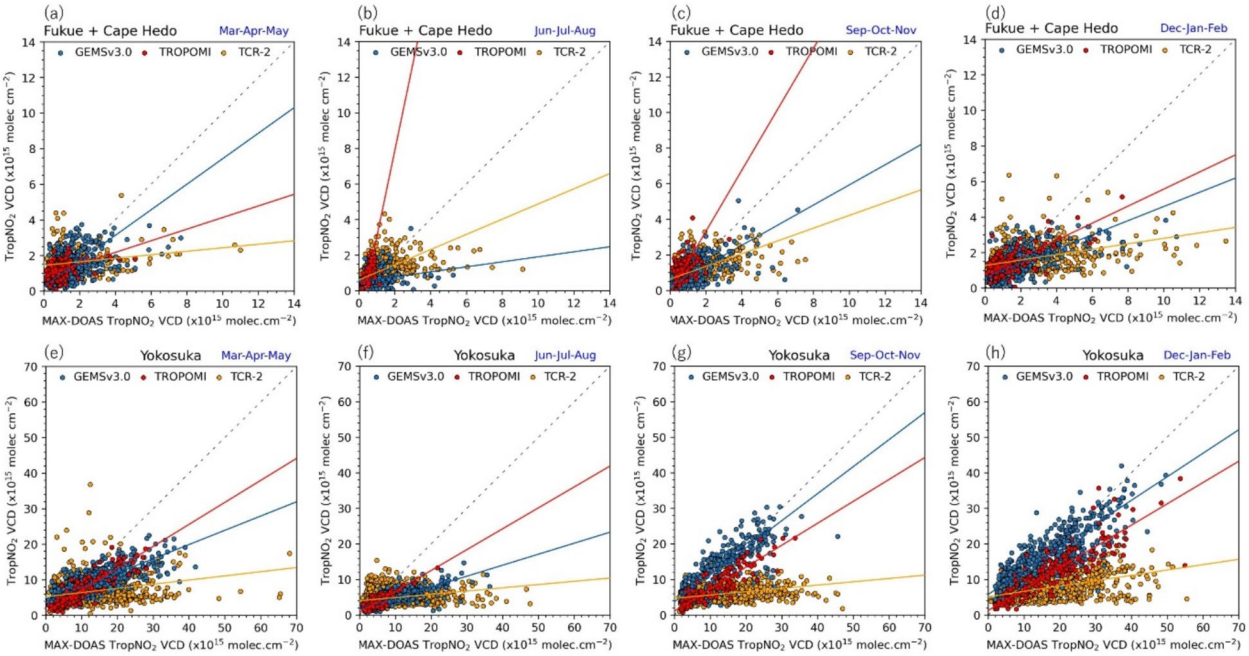

Fig. 5 Scatter plots for hourly $TropNO_2$ VCD data at Fukue + Cape Hedo and Yokosuka shown by seasons. Data from GEMS v3.0 (blue), TROPOMI (red), and TCR-2 (yellow) versus MAX-DOAS are presented across seasons: spring (a, e), summer (b, f), autumn (c, g), and winter (d, h). Data over all of the daytime are used when plotting GEMSv3.0 and TCR-2. Statistical metrics of these plots are displayed in Tables 4 and S1. All analyses have P values < 0.05. It should be noted that different x/y ranges between a – d and e – h are used

2 – 3%). However, the regression slope is worse in summer. The performance differences of GEMS and TCR-2 between diurnal data and data at TROPOMI overpass time highlight the importance of the bimodal morning and afternoon NO_2 peaks for analyses, while also underscore the challenges that satellite instruments face in accurately capturing near-surface NO_2 at high SZA compared to ground-based instruments.

Table 4 Similar to Table 3 but for Yokosuka for each season (in accordance with Fig. 5e to h)

	GEMSv3	TROPOMI	TCR-2	GEMSv3	TROPOMI	TCR-2
	March–April–May			June–July–August		
a	3.89 ± 0.20	0.84 ± 0.29	5.23 ± 0.19	1.64 ± 0.15	0.75 ± 0.19	3.40 ± 0.07
b	0.40 ± 0.01	0.62 ± 0.03	0.12 ± 0.01	0.31 ± 0.01	0.59 ± 0.03	0.09 ± 0.01
R	0.78	0.87	0.26	0.79	0.84	0.29
N	543	151	818	308	104	1432
MBE	−3.79	−2.64	−5.03	−4.78	−1.06	−2.89
NMB (%)	−29.5	−28.9	−43.2	−51.2	−24.1	−38.1
	September–October–November			December–January–February		
a	3.70 ± 0.47	1.11 ± 0.36	4.70 ± 0.16	5.80 ± 0.41	1.28 ± 0.53	5.14 ± 0.24
b	0.76 ± 0.03	0.62 ± 0.03	0.09 ± 0.01	0.66 ± 0.02	0.60 ± 0.03	0.15 ± 0.01
R	0.80	0.89	0.35	0.80	0.86	0.44
N	291	127	650	460	179	629
MBE	0.47	−3.27	−8.40	−0.08	−5.89	−10.72
NMB (%)	3.5	−28.6	−58.2	−0.4	−32.9	−57.4

3.1.2 Diurnal variations

As illustrated in Fig. 6, the dataset reveals diurnal variations in TropNO_2 VCD at the three sites across different seasons. There is a high degree of similarity between GEMS and MAX-DOAS diurnal variations in TropNO_2 VCD, particularly during the spring season, when both capture a morning peak just before noon, followed by a midday reduction. This behavior resembles the diurnal patterns observed in Beijing and Seoul (Yang et al. 2024; Edwards et al. 2024). In spring, the early morning structure observed by MAX-DOAS is also parallel in the GEMS data. During autumn and winter, the midday pattern remains consistent between the two datasets at Fukue and Cape Hedo from ~ 8 AM to ~ 3 PM. MAX-DOAS observations at Yokosuka and Fukue show consistent midday NO_2 reductions across all seasons, and partially at Cape Hedo. GEMS also detects this reduction especially at Fukue, except in summer. TROPOMI also partially reflect this reduction at all three sites, despite its limited temporal coverage. In summer, GEMS successfully represents the midday low levels at Cape Hedo. These behaviors demonstrate the capacity of GEMS v3.0 to generally capture diurnal variations in TropNO_2 VCD, even within relatively clean regions such as Fukue and Cape Hedo.

Exceptions in GEMS that deviate from the typical MAX-DOAS diurnal structure include early morning patterns, especially the flat morning profiles in summer, and the absence of afternoon data at Yokosuka. The GEMS data available for Yokosuka only encompasses the morning period, as the site lies outside the GEMS scan areas during afternoon. The flat summer morning profiles observed in GEMS at all three sites contrast with the NO_2 enhancements captured by MAX-DOAS, suggesting limited sensitivity to changes in early morning NO_2 levels. This flat morning pattern in summer is not observed at South Korean stations in the scientific GEMS IUP-UB product (Seo et al. 2025). In summer, the HE and HK scan modes are shorter (one hour each) and transition quicker than in other seasons. At Cape Hedo in summer, the HE and HK scan modes also have a narrower range of TropNO_2 VCD values than in autumn (see Figure S4). Therefore, the deviations in the diurnal variation of the GEMS data compared to MAX-DOAS and TCR-2 may be due to indirect factors related to the GEMS scan sequence, such as data retrieval sensitivity, despite higher morning values and clear midday reductions present in the MAX-DOAS data and partial visible in the TCR-2 data.

As illustrated in Figure S2, the diurnal ratio plots of GEMS v3.0 compared to MAX-DOAS demonstrate nearly constant ratios over the day within one season, but these can differ significantly between seasons, from 0.5 to 1.5, especially for Yokosuka (plots b to d). The GEMS/MAX-DOAS ratios in version 3.0 show an apparent improvement compared to version 2.0 for the autumn and winter periods at Yokosuka, while the ratios are more constant over the day in v3.0 but with larger biases in summer and spring, including around noon (see Figure S2a and b). However, low ratios persist at 7 AM in autumn at Yokosuka and Fukue (see also in Fig. 6c and g), which is possibly due to the limited number of GEMS data available at this early hour (e.g., only 12 data counts at 7 AM for Yokosuka in autumn vs. ~ 80 in spring and summer). Therefore, the recommendation is to refrain from using these data, even for v3.0. Lower ratios in summer are observed at Yokosuka, Fukue, and in the morning at Cape Hedo, resulting from the

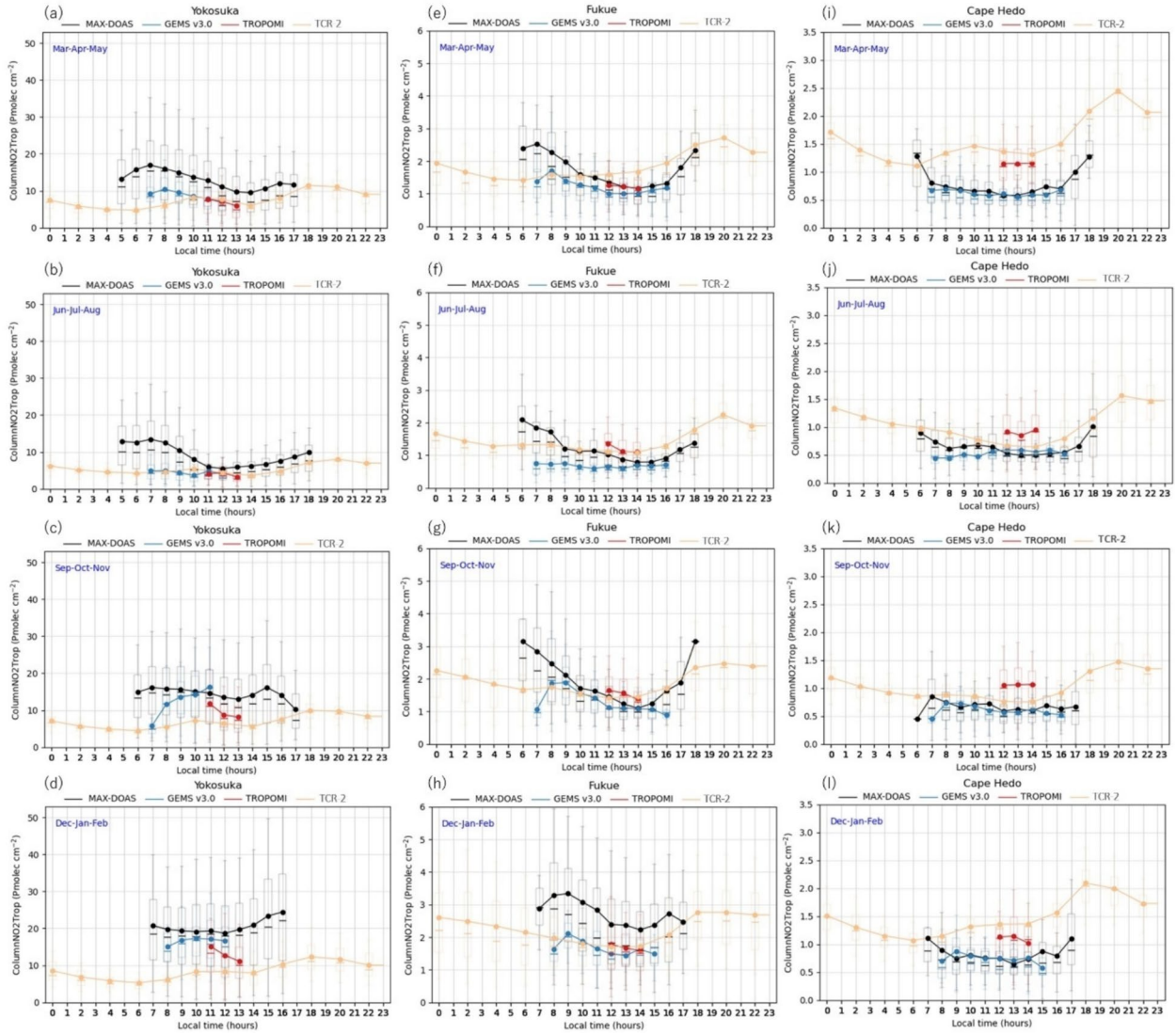

Fig. 6 Diurnal variations of TropNO_2 VCD at three stations are presented. Data from MAX-DOAS (black), GEMS (blue), TROPOMI (red), and TCR-2 (yellow) at Yokosuka (first column), Fukue (second column), and Cape Hedo (third column) are shown. Horizontal connected lines display the hourly mean values of each dataset in respective colors. The boxes represent the interquartile range (IQR), and the whiskers extend to the smallest and largest values within 1.5 times the IQR from the quartiles. Dashed lines show the medium values of each hourly dataset

morning flat patterns of GEMS, as previously explained (see Figs. 6 and S4a). Furthermore, as illustrated in Fig. 6, the midday TropNO_2 VCD levels measured by TROPOMI are mostly captured by MAX-DOAS and GEMS at Yokosuka and Fukue (Fig. 6a–h). However, these levels tend to be higher than those measured at Cape Hedo (Fig. 6i–l). This finding suggests that the GEMS NO_2 product may offer certain advantages for studying cleaner sites in comparison to TROPOMI.

Diurnal variations in TCR-2 at Fukue and Cape Hedo indicate elevated NO_2 levels during the night-time hours (6–8 PM), with a gradual increase from the afternoon. These variations cannot be captured by GEMS due to the observation schedule, and are only partially captured by MAX-DOAS. During the spring season, when continental outflow is prevalent, elevated NO_2 levels are observed at Cape Hedo in both TCR-2 data and partially MAX-DOAS measurements ($\sim 1.5 \times 10^{15}$ molecules/cm^2). These concentrations are comparable to those recorded in Fukue and are likely influenced by rapid transport from inland East Asia, a region with high NO_x emissions (Takashima et al. 2011; Figure S3). The significant decline in NO_2 observed by MAX-DOAS and GEMS from morning to noon at Fukue, but

only partially at Cape Hedo, appears as a similar pattern across both sites in the TCR-2 data. This likely reflects the limited ability of TCR-2 to resolve regional variability between the two locations, given that Fukue is with greater proximity to emission sources (e.g., Korea and China). In general, the spring NO_2 levels in TCR-2 data were higher than in MAX-DOAS or GEMS data, suggesting that the transport dynamics may not be represented well with the coarse resolution of TCR-2. During summer and autumn, with more influence from oceanic air masses, both TCR-2 and GEMS effectively capture the midday NO_2 levels at Cape Hedo (Fig. 6j and k), as observed by MAX-DOAS, underscoring their utility for analyzing photochemical processes in this remote region. This distinctive feature will be examined in further detail in Sect. 3.2.

3.1.3 Vertical distributions

In this section, a comparison is made between the vertical profiles of daytime NO_2 levels from TCR-2 and GEMS with those from MAX-DOAS at Cape Hedo. The vertical profiles of NO_2 mixing ratios are retrieved as described in Sect. 2.6. This comparison highlights the strong performance of TCR-2 in reference to MAX-DOAS. It is important to note that the typical degrees of freedom for signal (DOFS) from MAX-DOAS are only 2–3 (Tirpitz et al. 2021), even when the uncertainties in the observed NO_2 slant column densities are small. Moreover, the GEMS vertical profiles were redistributed from the TropNO_2 VCD according to the assumed vertical profile shape from GEOS-Chem. The primary aim of this investigation is to verify the qualitative agreement between the vertical profiles of the datasets. Section 3.2 examines the diurnal variation of the near-surface layer at the background site of Cape Hedo. Due to variations in emissions at the more polluted Fukue site, this section focuses solely on the vertical NO_2 distribution during midday hours (10 AM–3 PM) at Cape Hedo. Vertical distributions of NO_2 at Fukue and Yokosuka can be found in Figure S8 in the Supplement.

As shown in Fig. 7, the TCR-2 reanalysis data exhibited a considerable degree of accuracy in capturing NO_2 concentrations ranging from ground level to approximately 1.5 km, as measured by MAX-DOAS at Cape Hedo. This accuracy was particularly evident in the near-surface layer (0–100 m) in summer, autumn, and partially in winter. The elevated concentrations of NO_2 below 1 km in TCR-2 in spring and winter, which persist throughout the day (Fig. 6i, l; Figure S3a, d), potentially reflect errors in the transport of emissions, likely stemming from the coarse resolution of TCR-2. Additionally, GEMS demonstrated reasonable agreement with MAX-DOAS in the near-surface layer (0–100 m) and above 500 m, as well as with TCR-2 in summer and autumn. However, GEMS tends to underestimate NO_2 concentrations compared to MAX-DOAS and TCR-2 within the 100–500 m altitude range at Cape Hedo. Meaningful quantitative transformation of the vertical profiles of GEMS data may require further algorithmic development to narrow the gap with observations. Nevertheless, the results for the near-surface layer underscore the potential of GEMS data to facilitate analysis, even in remote regions.

3.2 Tracing midday NO_x reduction in the remote background environment

Given the strong performance of TCR-2 data during midday in summer and autumn, this section analyzes potential NO_2 loss processes observed by MAX-DOAS

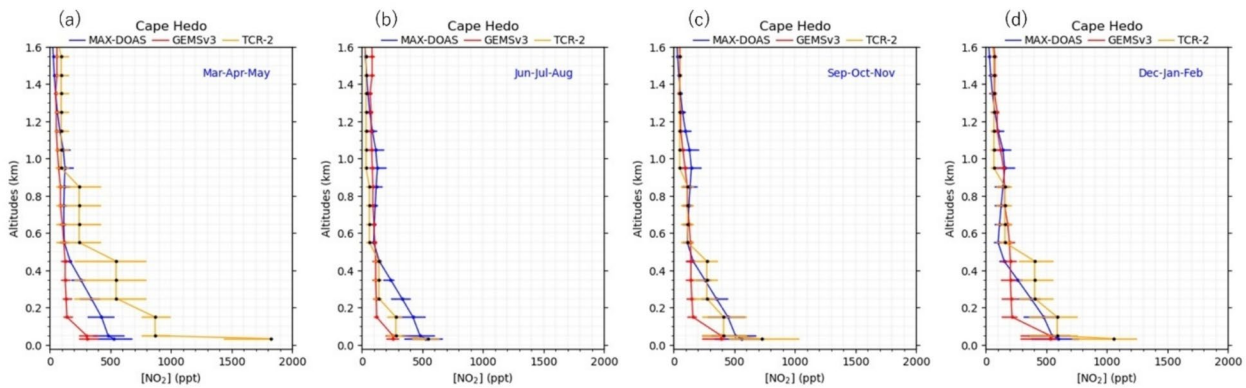

Fig. 7 Vertical profiles of midday NO_2 levels (ppt) from 10 AM–3 PM at Cape Hedo. Data from MAX-DOAS (blue), GEMS (red), and TCR-2 (yellow) are scaled to MAX-DOAS vertical height profile. Vertical lines show mean values at each altitude in respective colors, with horizontal lines indicating Interquartile Range (IQR) × 0.75 ranges

and partially by the GEMS satellite during the midday period (10 AM – 3 PM) at Cape Hedo. Grid data from TCR-2 and data from box-model simulations are utilized to investigate NO_2 loss pathways in a clean environment and calculate their relative contributions to the midday NO_x reduction.

Figure 8 presents the midday variations of NO_2 (or NO_x) and their decay rates in the near-surface layer (0–100 m) at Cape Hedo during summer and autumn. It should be noted that all datasets have been filtered for common days and hours. NO_2 levels from TCR-2 closely match the midday concentrations measured by MAX-DOAS in summer (380–500 ppt by TCR-2 and 400–540 ppt by MAX-DOAS) and autumn (400–660 ppt by TCR-2 and 450–600 ppt by MAX-DOAS), resulting in similar NO_2 decay curves. NO_2 levels from the GEMS show a clear decrease (from 400 to 220 ppt) between 10 AM and 3 PM during the autumn months. This decrease in NO_2 levels from the GEMS is consistent with the observed patterns in the MAX-DOAS and TCR-2 data. The parallel decay curves of the MAX-DOAS and TCR-2 NO_2 and NO_x in both summer and autumn suggest that the photochemical mechanism in the TCR-2 is also valid. The comparable decay of NO_x and NO_2 in the TCR-2 suggests that NO_2-to-NO partitioning played a negligible role. During the summer months, however, the GEMS data reveal no decrease in NO_2 levels between 10 AM and 3 PM at Cape Hedo. This may be related to the indirect influence of the scan sequence from morning to afternoon on retrieval sensitivities, as well as the insufficient near-surface data available between 10 AM and 1 PM (see Sect. 3.1.2 and Figure S4a). Additionally, the statistical conversion may be insufficient to fully capture the decreasing signal from the limited 2.5 year dataset. During autumn, GEMS exhibits a more pronounced diurnal decline, with a decay rate that closely aligns with MAX-DOAS and TCR measurements.

Table 2 shows the midday-averaged NO_2 and NO_x decay rates near the surface, which have been derived from the exponential curve fitting in Fig. 8. During the autumn, the NO_2 decay rates derived from MAX-DOAS exhibited a close correspondence with those from TCR-2 ($\tau = 21 \pm 5$h vs. 22 ± 20h). The NO_2 decay rate derived from GEMS (16 ± 10h) shows improved convergence with both MAX-DOAS and TCR-2 when GEMS data within $\pm 0.2°$ are allowed, compared to $\pm 0.05°$. This consistency may be attributed to the increased data availability and statistical convergence in this remote region with low NO_2 levels (see Figure S4d). The large uncertainty ranges in the autumn decay rates of TCR-2 and GEMS account for the greater variability observed in these datasets in Fig. 8b. During the summer months, the NO_2 decay rate as estimated by MAX-DOAS showed a reduced agreement with TCR-2 ($\tau = 17 \pm 8$h vs. 30 ± 8h) in comparison to autumn.

The simulated diurnal variations of NO_2, NO, and NO_x, as illustrated in Figure S6a, exhibit midday reductions in NO_2 and NO_x, which broadly align with trends observed in TCR-2 and other datasets. The box-model NO_x budget analysis identifies four key pathways driving midday NO_2

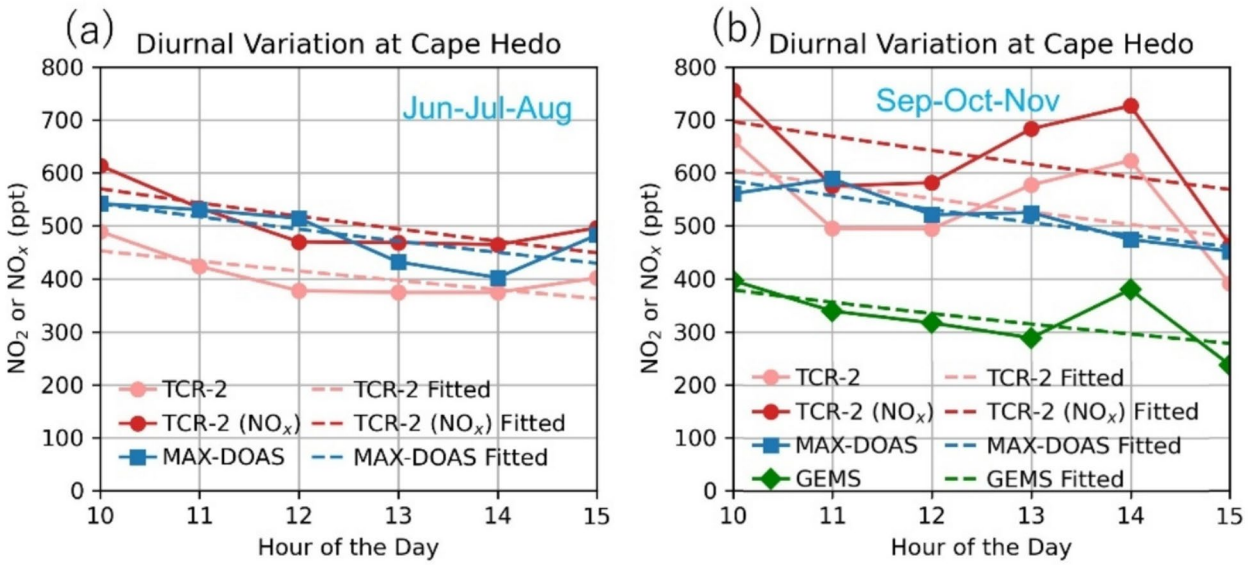

Fig. 8 Midday variations (10 AM – 3 PM) of NO_2 (or NO_x) near the surface (~ 100 m) at Cape Hedo during summer (**a**) and autumn (**b**). Solid lines represent hourly data, while dashed lines indicate exponential decay curve fitting. The data sources include TCR-2 (NO_x in red, NO_2 in pink), MAX-DOAS (blue), and GEMS (green), with GEMS data extracted within a 0.2° radius around the MAX-DOAS site

loss (10 AM–3 PM) (Figure S6b), with OH reactions dominating as the primary loss mechanism, contributing approximately 80% at 10 AM and increasing to nearly 90% by early afternoon. This primary loss mechanism is consistent with the theoretical framework proposed by Kanaya et al. (2014). It is clear that alternative pathways are significantly less competitive when compared with this OH-driven loss process. Residual NO_2-to-NO partitioning contributes 5–15%, while PAN decomposition and reformation account for a maximum of 10%, peaking before noon and diminishing significantly in the afternoon. Another pathway, the net contribution from the thermal decomposition of peroxynitric acid (HNO_4), was minimal at 1–2%. However, the dominant loss pathway identified in this analysis may not be applicable to other sites, given that diurnal variations in emissions are much more significant in urban areas. Further details on the box model simulation, including oxidant mixing ratios and the chemical decay rates of NO_2, are provided in Figure S7. Further investigation is necessary to establish a quantitative relationship between the observed decay rates and the 1/k[OH] rate under conditions involving additional NO_2 sources and sinks, as well as in/outfluxes driven by advection. The net PAN-NO_x flux has to be re-evaluated with the transport term in the 3D model. The agreement between the GEMS data and the MAX-DOAS and TCR-2 data in terms of the decrease in midday NO_2 warrants the potential of GEMS for future chemical budget analyses in remote regions.

4 Conclusions

This paper validated the TropNO_2 VCD data from GEMS and TCR-2 against the MAX-DOAS and TROPOMI data at three sites in Japan: Yokosuka (urban), Fukue (rural-remote), and Cape Hedo (remote). GEMS v3.0 showed a significant improvement in agreement with MAX-DOAS compared to v2.0, particularly at Fukue and Cape Hedo. The normalized mean bias was dramatically reduced from 142–319% to 8–18%. GEMS v3.0 performed particularly well in autumn and winter ($R = 0.80$ at Yokosuka; $R = 0.60$–0.66 at Fukue and Cape Hedo), exhibiting a slight positive bias in autumn at Yokosuka (NMB = 3.5%) while negative biases in winter (NMB = -0.4%), notably in spring (NMB = -29.5%) and summer (NMB = -51.2%). GEMS v3.0 generally reproduced the diurnal variations in TropNO_2 VCD in relatively clean regions like Fukue and Cape Hedo. Notably, it captured the midday TropNO_2 VCD observed by MAX-DOAS at Cape Hedo more accurately than TROPOMI, demonstrating its advantages over TROPOMI for studying low-NO_2 environments.

Due to the coarse spatial resolution of TCR-2 reanalysis data, a meaningful comparison with MAX-DOAS at Yokosuka, an urban site, was not feasible. However, at the background site of Cape Hedo, TCR-2 displayed a significantly lower bias relative to MAX-DOAS compared to TROPOMI (NMB = 38% vs. 87%). Aggregating TROPOMI TropNO_2 VCD data to the same 1.1° resolution as the TCR-2 data improves comparison accuracy with TCR-2, yielding significant increases in the correlation coefficients and the slope values across all three sites. Moreover, both the TCR-2 and GEMS data showed strong alignment with the MAX-DOAS data in terms of capturing low NO_2 levels at midday in summer and NO_2 reductions at midday in autumn at Cape Hedo. This underscored their utility in analyzing chemical loss processes, even within very low NO_2 concentration ranges. For the near-surface layer (0–100 m) at Cape Hedo, NO_2 decay rates were comparable across MAX-DOAS ($\tau = 21 \pm 5$h), TCR-2 ($\tau = 22 \pm 20$h), and GEMS with broader coverage ($\pm 0.2°$) (16 ± 10h). The box-model simulation indicated that the NO_2 + OH reaction was the predominant pathway for NO_x loss, while PAN-related processes had only a minimal net impact. Quantitative relationship between decay rates and chemical lifetime must be a target of future studies. Moreover, future versions of GEMS should incorporate algorithmic improvements to enable more precise data retrieval in the near-surface layer during spring and summer.

Abbreviations

SZA	Solar zenith angles
CAMS	Copernicus atmosphere monitoring service
CHASER	Chemical atmospheric general circulation model for study of atmospheric environment and radiative forcing
FC	Full central
FW	Full west
GEMS	Geostationary environment monitoring spectrometer
GEOS-Chem	Goddard earth observing system-chem model
GES-DISC	NASA goddard earth sciences data and information services center
HE	Half east
HK	Half Korea
IQR	Interquartile range
MAX-DOAS	Multi-axis differential optical absorption spectroscopy
MIROC-ESM	Model for interdisciplinary research on climate – earth system model
MIROC	Model for interdisciplinary research on climate
PA	Peroxyacetyl
PAN	Peroxyacetyl nitrate
TCR-2	Tropospheric chemistry reanalysis version 2
TROPOMI	Tropospheric monitoring instrument
TropNO_2 VCD	Tropospheric NO_2 vertical column density
MBE	Mean bias error
NMB	Normalized mean bias

Supplementary Information

The online version contains supplementary material available at https://doi.org/10.1186/s40645-026-00813-y.

Additional file 1.

Acknowledgement
We sincerely appreciate the free availability of Sentinel-5P TROPOMI NO_2 retrievals, which have been invaluable for this study.

Author contributions
PTMH analyzed the data and wrote the manuscript. YK conducted MAX-DOAS observations at Yokosuka and Fukue, collaborated with data owners, provided the processed observational data, helped in the interpretation, and supervised the analysis. TS composed the TCR-2 dataset and assisted in the analysis of both TCR-2 and the box-model results. HT conducted MAX-DOAS observations at Cape Hedo. KS developed the CHASER model, including its box-model version, and has applied it to compile the TCR-2 dataset. YC supported the GEMS data validation using the MAX-DOAS observations. LC, HL, HH, and JK developed and operated GEMS satellite and algorithms, providing the GEMS data to validation teams. All authors helped in the discussions and approved the final manuscript.

Funding
This research was performed by the Environment Research and Technology Development Fund (JPMEERF20222001 and JPMEERF24S12200) of the Environmental Restoration and Conservation Agency provided by Ministry of the Environment of Japan. This research was also supported by the NIES-JAMSTEC-NICT collaboration framework regarding GOSAT-GW satellite observations.

Data availability
The GEMS version 3.0 TropNO_2 VCD data are available from NIER, Korea, https://nesc.nier.go.kr/en/html/index.do. The TROPOMI data are available at https://www.temis.nl/airpollution/no2col/no2regio_tropomi.php. The MAX-DOAS data are available from https://www.jamstec.go.jp/egcr/e/atmos/observation/maxdoashp/. The TCR-2 data are available from https://doi.org/10.25966/9qgv-fe81.

Declarations

Competing interests
The authors declare that they have no competing interest.

Author details
[1]Research Institute for Global Change, JAMSTEC, 3173-25 Showa-machi, Kanazawa-ku, Yokohama, Kanagawa 236–0001, Japan. [2]Faculty of Science, Fukuoka University, 8-19-1 Nanakuma, Jonan, Fukuoka 814-0180, Japan. [3]Nagoya University, Furo-cho, Chikusa-ku, Aichi, Nagoya 464-8601, Japan. [4]Hankuk University of Foreign Studies (HUFS), Yongin 17035, Republic of Korea. [5]National Institute of Environmental Research, Incheon, Republic of Korea. [6]Pukyong National University, Busan, Republic of Korea. [7]Yonsei University, Seoul, Republic of Korea.

Received: 29 April 2025 Accepted: 15 March 2026
Published online: 01 April 2026

References

Boersma KF, Eskes H, Richter A, De Smedt I, Lorente A, Beirle S, Van Geffen J, Peters E, Van Roozen dael M, and Wagner T (2017): QA4ECV NO2 tropospheric and stratospheric vertical column data from OMI (Version 1.1), Royal Netherlands Meteorological Institute (KNMI), https://doi.org/10.21944/qa4ecv-no2-omi-v1.1 (last Accessed: 20 April 2020)

Burrows JP, Weber M, Buchwitz M, Rozanov V, Ladstätter-Weißenmayer A, Richter A, DeBeek R, Hoogen R, Bramstedt K, Eichmann K-U, Eisinger M, Perner D (1999) The global ozone monitoring experiment (GOME): mission concept and first scientific results. J Atmos Sci 56:151–175. https://doi.org/10.1175/1520-0469(1999)056%3c0151:TGOMEG%3e2.0.CO;2

Choi Y, Kanaya Y, Takashima H, Irie H, Park K, Chong J (2021) Long-term variation in the tropospheric nitrogen dioxide vertical column density over Korea and Japan from the MAX-DOAS network, 2007–2017. Remote Sens 13:1937. https://doi.org/10.3390/rs13101937

Cifuentes F, Eskes H, Dammers E, Bryan C, Boersma F (2025) Accurate space-based NO_x emission estimates with the flux divergence approach require fine-scale model information on local oxidation chemistry and profile shapes. Geosci Model Dev 18:621–649. https://doi.org/10.5194/gmd-18-621-2025

Coates J, Butler TM (2015) A comparison of chemical mechanisms using tagged ozone production potential (TOPP) analysis. Atmos Chem Phys 15:8795–8808. https://doi.org/10.5194/acp-15-8795-2015

Deeter MN, Edwards DP, Francis GL, Gille JC, Martínez-Alonso S, Worden HM, Sweeney C (2017) A climate-scale satellite record for carbon monoxide: the MOPITT Version 7 product. Atmos Meas Tech 10:2533–2555. https://doi.org/10.5194/amt-10-2533-2017

Douros J, Eskes H, van Geffen J, Boersma KF, Compernolle S, Pinardi G, Blechschmidt A-M, Peuch V-H, Colette A, Veefkind P (2023) Comparing Sentinel-5P TROPOMI NO2 column observations with the CAMS regional air quality ensemble. Geosci Model Dev 16:509–534. https://doi.org/10.5194/gmd-16-509-2023

East JD, Henderson BH, Napelenok SL, Koplitz SN, Sarwar G, Gilliam R, Lenzen A, Tong DQ, Pierce RB, Garcia-Menendez F (2022) Inferring and evaluating satellite-based constraints on NO_x emissions estimates in air quality simulations. Atmos Chem Phys 22:15981–16001. https://doi.org/10.5194/acp-22-15981-2022

Edwards DP, Martínez-Alonso S, Jo DS, Ortega I, Emmons LK, Orlando JJ, Worden HM, Kim J, Lee H, Park J, Hong H (2024) Quantifying the diurnal variation in atmospheric NO_2 from Geostationary Environment Monitoring Spectrometer (GEMS) observations. Atmos Chem Phys 24:8943–8961. https://doi.org/10.5194/acp-24-8943-2024

Ghahremanloo M, Choi Y, Singh D (2024) Deep learning bias correction of GEMS tropospheric NO_2: a comparative validation of NO_2 from GEMS and TROPOMI using Pandora observations. Environ Int 190:0160–4120. https://doi.org/10.1016/j.envint.2024.108818

Ha PTM, Matsuda R, Kanaya Y, Taketani F, Sudo K (2021) Effects of heterogeneous reactions on tropospheric chemistry: A global simulation with the chemistry–climate model CHASER V4.0. Geosci Model Dev 14:3813–3841. https://doi.org/10.5194/gmd-14-3813-2021

Ha PTM, Kanaya Y, Taketani F, Andrés Hernández MD, Schreiner B, Pfeilsticker K, Sudo K (2023) Implementation of HONO into the chemistry–climate model CHASER (V4.0): roles in tropospheric chemistry. Geosci Model Dev 16:927–960. https://doi.org/10.5194/gmd-16-927-2023

He Y, Hoque HMS, Sudo K (2022) Introducing new lightning schemes into the CHASER (MIROC) chemistry–climate model. Geosci Model Dev 15:5627–5650. https://doi.org/10.5194/gmd-15-5627-2022

Honda MC, Wakita M, Matsumoto K, Fujiki T, Siswanto E, Sasaoka K, Kawakami H, Mino Y, Sukigara C, Kitamura M, Sasai Y, Smith SL, Hashioka T, Yoshikawa C, Kimoto K, Watanabe S, Kobari T, Nagata T, Hamasaki K, Kaneko R, Uchimiya M, Fukuda H, Abe O, Saino T (2017) Comparison of carbon cycle between the western Pacific subarctic and subtropical time-series stations: highlights of the K2S1 project. J Oceanogr 73:647–667. https://doi.org/10.1007/s10872-017-0423-3

Hoque HMS, Sudo K, Irie H, He Y, Khan MF (2024) Evaluating CHASER V4.0 global formaldehyde (HCHO) simulations using satellite, aircraft, and ground-based remote-sensing observations. Geosci Model Dev 17:5545–5571. https://doi.org/10.5194/gmd-17-5545-2024

Hunt BR, Kostelich EJ, Szunyogh I (2007) Efficient data assimilation for spatiotemporal chaos: A local ensemble transform Kalman filter. Physica D 230:112–126. https://doi.org/10.1016/j.physd.2006.11.008

Jaeglé L, Steinberger L, Martin RV, Chance K (2005) Global partitioning of NO_x sources using satellite observations: Relative roles of fossil fuel combustion, biomass burning and soil emissions. Faraday Dis. https://doi.org/10.1039/B502128F

Kanaya Y, Irie H, Takashima H, Iwabuchi H, Akimoto H, Sudo K, Gu M, Chong J, Kim YJ, Lee H, Li A, Si F, Xu J, Xie P-H, Liu W-Q, Dzhola A, Postylyakov O, Ivanov V, Grechko E, Terpugova S, Panchenko M (2014) Long-term MAX-DOAS network observations of NO_2 in Russia and Asia (MADRAS) during the period 2007–2012: Instrumentation, elucidation of climatology, and comparisons with OMI satellite observations and global model simulations. Atmos Chem Phys 14:7909–7927. https://doi.org/10.5194/acp-14-7909-2014

Kanaya Y, Miyazaki K, Taketani F, Miyakawa T, Takashima H, Komazaki Y, Pan X, Kato S, Sudo K, Sekiya T, Inoue J, Sato K, Oshima K (2019) Ozone and carbon monoxide observations over open oceans on R/V Mirai from 67 S to 75 N during 2012 to 2017: testing global chemical reanalysis in terms of Arctic processes, low ozone levels at low latitudes, and pollution

transport. Atmos Chem Phys 19:7233–7254. https://doi.org/10.5194/acp-19-7233-2019

Kasibhatla P, Sherwen T, Evans MJ, Carpenter LJ, Reed C, Alexander B, Chen Q, Sulprizio MP, Lee JD, Read KA, Bloss W, Crilley LR, Keene WC, Pszenny AAP, Hodzic A (2018) Global impact of nitrate photolysis in sea-salt aerosol on NO_x, OH, and O_3 in the marine boundary layer. Atmos Chem Phys 18:11185–11203. https://doi.org/10.5194/acp-18-11185-2018

Kim J, Jeong U, Ahn MH, Kim JH, Park RJ, Lee H, Song CH, Choi YS, Lee KH, Yoo JM, Jeong MJ, Park SK, Lee KM, Song CK, Kim SW, Kim YJ, Kim SW, Kim M, Go S, Liu X, Chance K, Miller CC, Al-Saadi J, Veihelmann B, Bhartia PK, Torres O, Abad GG, Haffner DP, Choi Y et al (2020) New era of air quality monitoring from Space: Geostationary environment monitoring spectrometer (GEMS). Bull Am Meteor Soc. https://doi.org/10.1175/BAMS-D-18-0013.1

Kim S, Kim D, Hong H, Chang L-S, Lee H, Kim D-R, Kim D, Yu J-A, Lee D, Jeong U, Song C-K, Kim S-W, Park SS, Kim J, Hanisco TF, Park J, Choi W, Lee K (2023) First-time comparison between NO_2 vertical columns from Geostationary Environmental Monitoring Spectrometer (GEMS) and Pandora measurements. Atmos Meas Tech 16:3959–3972. https://doi.org/10.5194/amt-16-3959-2023

Lange K, Richter A, Bösch T, Zilker B, Latsch M, Behrens LK, Okafor CM, Bösch H, Burrows JP, Merlaud A, Pinardi G, Fayt C, Friedrich MM, Dimitropoulou E, Van Roozendael M, Ziegler S, Ripperger-Lukosiunaite S, Kuhn L, Lauster B, Wagner T, Hong H, Kim D, Chang L-S, Bae K, Song C-K, Park J-U, Lee H (2024) Validation of GEMS tropospheric NO_2 columns and their diurnal variation with ground-based DOAS measurements. Atmos Meas Tech 17:6315–6344. https://doi.org/10.5194/amt-17-6315-2024

Lee H, Park J, Jung Y, Hong H. Geostationary Environment, Monitoring Spectrometer (GEMS), Algorithm Theoretical Basis Document, NO_2 Retrieval Algorithm, (October 2024) Environmental Satellite Center, National Institute of Environmental Research, Ministry of Environment, https://nesc.nier.go.kr/en/html/satellite/doc/doc.do, last Accessed: 15/4/2025

Li C, Joiner J, Krotkov NA, Bhartia PK (2013) A fast and sensitive new satellite SO_2 retrieval algorithm based on principal component analysis: application to the ozone monitoring instrument. Geophys Res Lett 40:6314–6318. https://doi.org/10.1002/2013GL058134

Livesey NJ, Read WG, Wagner PA, Froidevaux L, Lambert A, Manney GL, Millán Valle LF, Pumphrey HC, Santee ML, Schwartz MJ, Wang S, Fuller RA, Jarnot RF, Knosp BW, Martinez E, and Lay RR (2018) Aura Microwave Limb Sounder (MLS) Version 4.2x Level2 data quality and description document. Tech rep, Jet Propul Lab, Pasadena, CA, tech Rep JPL D33509 Rev D, https://mls.jpl.nasa.gov/data/v4-2_data_quality_document.pdf (last Accessed: 1 August 2024)

Miyazaki K, Eskes HJ, Sudo K (2015) A tropospheric chemistry reanalysis for the years 2005–2012 based on an assimilation of OMI, MLS, TES, and MOPITT satellite data. Atmos Chem Phys 15:8315–8348. https://doi.org/10.5194/acp-15-8315-2015

Miyazaki K, Bowman K, Sekiya T, Eskes H, Boersma F, Worden H, Livesey N, Payne VH, Sudo K, Kanaya Y, Takigawa M, Ogochi K (2019a) Chemical reanalysis products. NASA DOIMS. https://doi.org/10.25966/9qgv-fe81

Miyazaki K, Sekiya T, Fu D, Bowman K, Kulawik S, Sudo K, Walker T, Kanaya Y, Takigawa M, Ogochi K, Eskes H, Boersma KF, Thompson AM, Gaubert B, Barre J, Emmons LK (2019b) Balance of emission and dynamical controls on ozone during the Korea-United States air quality campaign from multiconstituent satellite data assimilation. J Geophys Res-Atmos 124:387–413. https://doi.org/10.1029/2018JD028912

Miyazaki K, Bowman K, Sekiya T, Eskes H, Boersma F, Worden H, Livesey N, Payne VH, Sudo K, Kanaya Y, Takigawa M, Ogochi K (2020) Updated tropospheric chemistry reanalysis and emission estimates, TCR-2, for 2005–2018. Earth Syst Sci Data 12:2223–2259. https://doi.org/10.5194/essd-12-2223-2020

Miyazaki K, Bowman K, Sekiya T, Takigawa M, Neu J, Sudo K, Osterman G, Eskes H (2021) Global tropospheric ozone responses to reduced NO_x emissions linked to the COVID-19 worldwide lockdowns. Sci Adv 7(24):eabf7460. https://doi.org/10.1126/sciadv.abf7460

Park J, Choi Y, Jung J, Lee K, Yeganeh AK (2024) First top-down diurnal adjustment to NO_x emissions inventory in Asia informed by the geostationary environment monitoring spectrometer (GEMS) tropospheric NO_2 columns. Sci Rep 14:24338. https://doi.org/10.1038/s41598-024-76223-1

Paulot F, Crounse JD, Kjaergaard HG, Kroll JH, Seinfeld JH, Wennberg PO (2009) Isoprene photooxidation: new insights into the production of acids and organic nitrates. Atmos Chem Phys 9:1479–1501. https://doi.org/10.5194/acp-9-1479-2009

Peters E, Wittrock F, Großmann K, Frieß U, Richter A, Burrows JP (2012) Formaldehyde and nitrogen dioxide over the remote western Pacific Ocean: SCIAMACHY and GOME-2 validation using ship-based MAX-DOAS observations. Atmos Chem Phys 12:11179–11197. https://doi.org/10.5194/acp-12-11179-2012

Platt U and Stutz J (2008) Evaluation of DOAS Spectra, Sensitivity, and Detection Limits. In: Platt U and Stutz J (2008) differential optical absorption spectroscopy, physics of earth and space environments, Springer-Verlag Berlin, https://doi.org/10.1007/978-3-540-75776-4-8.

Sekiya T, Miyazaki K, Ogochi K, Sudo K, Takigawa M (2018) Global high-resolution simulations of tropospheric nitrogen dioxide using CHASER V4.0. Geosci Model Dev 11:959–988. https://doi.org/10.5194/gmd-11-959-2018

Sekiya T, Miyazaki K, Eskes H, Sudo K, Takigawa M, Kanaya Y (2022) A comparison of the impact of TROPOMI and OMI tropospheric NO_2 on global chemical data assimilation. Atmos Meas Tech 15:1703–1728. https://doi.org/10.5194/amt-15-1703-2022

Seo S, Kim S-W, Kim K-M, Richter A, Lange K, Burrows JP, Park J, Hong H, Lee H, Jeong U, Woo J-H, Kim J (2025) Diurnal variations of NO_2 tropospheric vertical column density over the Seoul metropolitan area from the Geostationary environment monitoring spectrometer (GEMS): seasonal differences and the influence of the a priori NO_2 profile. Atmos Meas Tech 18:115–128. https://doi.org/10.5194/amt-18-115-2025

Stone D, Evans MJ, Edwards PM, Commane R, Ingham T, Rickard AR, Brookes DM, Hopkins J, Leigh RJ, Lewis AC, Monks PS, Oram D, Reeves CE, Stewart D, Heard DE (2011) Isoprene oxidation mechanisms: measurements and modelling of OH and HO_2 over a South-East Asian tropical rainforest during the OP3 field campaign. Atmos Chem Phys 11:6749–6771. https://doi.org/10.5194/acp-11-6749-2011

Sudo K, Akimoto H (2007) Global source attribution of tropospheric ozone: long-range transport from various source regions. J Geophys Res Atmos 112:D12302. https://doi.org/10.1029/2006JD007992

Sudo K, Takahashi M, Kurokawa JI, Akimoto H (2002) CHASER: a global chemical model of the troposphere 1. model description. J Geophys Res Atmos 107(D17):4339. https://doi.org/10.1029/2001JD001113

Takashima H, Irie H, Kanaya Y, Akimoto H (2011) Enhanced NO_2 at Okinawa Island, Japan caused by rapid air-mass transport from China as observed by MAX-DOAS. Atmos Environ 45:2593–2597. https://doi.org/10.1016/j.atmosenv.2010.10.055

Tirpitz J-L, Frieß U, Hendrick F, Alberti C, Allaart M, Apituley A, Bais A, Beirle S, Berkhout S, Bognar K, Bösch T, Bruchkouski I, Cede A, Chan KL, den Hoed M, Donner S, Drosoglou T, Fayt C, Friedrich MM, Frumau A, Gast L, Gielen C, Gomez-Martín L, Hao N, Hensen A, Henzing B, Hermans C, Jin J, Kreher K, Kuhn J et al (2021) Intercomparison of MAX-DOAS vertical profile retrieval algorithms: studies on field data from the CINDI-2 campaign. Atmos Meas Tech 14:1–35. https://doi.org/10.5194/amt-14-1-2021

Van Geffen JHGM, Eskes HJ, Compernolle S, Pinardi G, Verhoelst T, Lambert J-C, Sneep M, ter Linden M, Ludewig A, Boersma KF, Veefkind JP (2022) Sentinel-5P TROPOMI NO_2 retrieval: impact of version v2.2 improvements and comparisons with OMI and ground-based data. Atmos Meas Tech 15:2037–2060. https://doi.org/10.5194/amt-15-2037-2022

Veefkind JP, Aben I, McMullan K, Forster H, de Vries J, Otter G, Claas J, Eskes HJ, de Haan JF, Kleipool Q, van Weele M, Hasekamp O, Hoogeveen R, Landgraf J, Snel R, Tol P, Ingmann P, Voors R, Kruizinge B, Vink R, Visser H, Levelt PF (2012) TROPOMI on the ESA Sentinel-5 Precursor: a GMES mission for global observations of the atmospheric composition for climate, air quality and ozone layer applications. Remote Sens Environ 120:70–83. https://doi.org/10.1016/j.rse.2011.09.027

Verhoelst T, Compernolle S, Pinardi G, Lambert J-C, Eskes HJ, Eichmann K-U, Fjæraa AM, Granville J, Niemeijer S, Cede A, Tiefengraber M, Hendrick F, Pazmiño A, Bais A, Bazureau A, Boersma KF, Bognar K, Dehn A, Donner S, Elokhov A, Gebetsberger M, Goutail F, Grutter de la Mora M, Gruzdev A, Gratsea M, Hansen GH, Irie H, Jepsen N, Kanaya Y, Karagkiozidis D et al (2021) Ground-based validation of the Copernicus Sentinel-5P TROPOMI NO_2 measurements with the NDACC ZSL-DOAS, MAX-DOAS and Pandonia global networks. Atmos Meas Tech 14:481–510. https://doi.org/10.5194/amt-14-481-2021

Wang P, Piters A, van Geffen J, Tuinder O, Stammes P, Kinne S (2020) Shipborne MAX-DOAS measurements for validation of TROPOMI NO_2

products. Atmos Meas Tech 13:1413–1426. https://doi.org/10.5194/amt-13-1413-2020

Watanabe S, Hajima T, Sudo K, Nagashima T, Takemura T, Okajima H, Nozawa T, Kawase H, Abe M, Yokohata T, Ise T, Sato H, Kato E, Takata K, Emori S, Kawamiya M (2011) MIROC-ESM 2010: model description and basic results of CMIP5-20c3m experiments. Geosci Model Dev 4:845–872. https://doi.org/10.5194/gmd-4-845-2011

Wolfe GM, Marvin MR, Roberts SJ, Travis KR, Liao J (2016) The framework for 0-D atmospheric modeling (F0AM) v3.1. Geosci Model Dev 9:3309–3319. https://doi.org/10.5194/gmd-9-3309-2016

Yamaguchi R, Kouketsu S, Kosugi N, Ishii M (2024) Global upper ocean dissolved oxygen budget for constraining the biological carbon pump. Commun Earth Environ 5:732. https://doi.org/10.1038/s43247-024-01886-7

Yang LH, Jacob DJ, Dang R, Oak YJ, Lin H, Kim J, Zhai S, Colombi NK, Pendergrass DC, Beaudry E, Shah V, Feng X, Yantosca RM, Chong H, Park J, Lee H, Lee W-J, Kim S, Kim E, Travis KR, Crawford JH, Liao H (2024) Interpreting Geostationary Environment Monitoring Spectrometer (GEMS) geostationary satellite observations of the diurnal variation in nitrogen dioxide (NO_2) over East Asia. Atmos Chem Phys 24:7027–7039. https://doi.org/10.5194/acp-24-7027-2024

Publisher's Note